Analysis of sensor signals shows turning on a lathe exhibits low-dimensional chaos

Satishmohan T. S. Bukkapatnam*
Department of Industrial and Manufacturing Engineering, The Pennsylvania State University, University Park, Pennsylvania 16802

Akhlesh Lakhtakia†
Department of Engineering Science and Mechanics, The Pennsylvania State University, University Park, Pennsylvania 16802

Soundar R. T. Kumara‡
Department of Industrial and Manufacturing Engineering, The Pennsylvania State University, University Park, Pennsylvania 16802

(Received 25 August 1994; revised manuscript received 11 May 1995)

The dynamics of the turning operation on a lathe is commonly assumed to be linear, stochastic, or chaotic without experimental verification. Here we report three independent approaches — two statistical tests and a Lyapunov exponents-based test — to establish the presence of low-dimensional chaos in the sensor signals from actual experiments on a lathe.

PACS number(s): 05.45.+b

I. INTRODUCTION

On-line, real-time quality control schemes are deemed essential for the production of high quality products. Given the trend for globalization of markets, it is imperative that such schemes be robust and help in producing good and consistent quality products. In order to develop these on-line, real-time quality control schemes for a manufacturing process, the process needs to be monitored, faults have to be diagnosed, and a real-time control action needs to be enforced *in situ*.

In this paper, we address the domains of monitoring and control. We focus on the turning operation — a material removal process performed on a lathe — because that operation is industrially ubiquitous, and is perhaps the most basic material removal operation [1]. Because of the simplicity of the turning operation, fundamental understanding of the machining process is acquired usually through experiments on a lathe, and is later extended to other machining operations such as milling, etc.

A schematic of the turning operation is shown in Fig. 1. A cylindrical workpiece is held in the chuck of a lathe and rotated about an axis. A rigidly held cutting tool is made to traverse along the axis of rotation. Material is removed from the surface of the workpiece to reduce its diameter. The main parameters of the turning operation are (i) cutting speed: the tangential velocity of the surface of the workpiece; (ii) feed: the axial distance moved by the tool for every complete rotation of the workpiece; and (iii) depth-of-cut: the thickness of the metal removed from the workpiece. Precise relationships connecting these parameters and the states of the turning operation have to be established in order to develop control systems.

However, turning dynamics is poorly understood. Early models for turning operation were developed on the assumption that its dynamics is linear [2]. Later models assumed linear dynamics contaminated with additive noise [3]. However, these models are inadequate especially for global characterization of the turning dynamics; one should therefore resort to nonlinear models. The observation of complex response from a nonlinear model of Grabec [4] has prompted speculation that the dynamics of the turning operation may be chaotic.

Nonlinear model-based control schemes have not been developed due to the lack of knowledge about the exact nature of nonlinearity. In addition, the mere identification and characterization of chaos in a process does not lead to a model and hence a control scheme. Even when the exact nature of nonlinearity and chaos is known, the chaos model may not be of much use in process control if the dimension of the attractor of the underlying process dynamics is not low [5]. Furthermore, control paradigms and schemes for chaotic processes are still in their infancy [6].

About two years ago, we began a systematic approach to apply the tools of chaos theory to turning operation characterization and control. We used Grabec's model and understood that numerical integration must be carefully done [7]. This is because the use of finite differences induces spurious dynamics which may not actually belong to the physical operation, this understanding being in agreement with Pachner's widely applicable nu-

*Internet: satish@marie.psu.edu
†Author to whom correspondence should be addressed. Internet: all@eclx.psu.edu
‡Internet: kumara@marie.psu.edu

 ©1995 The American Physical Society

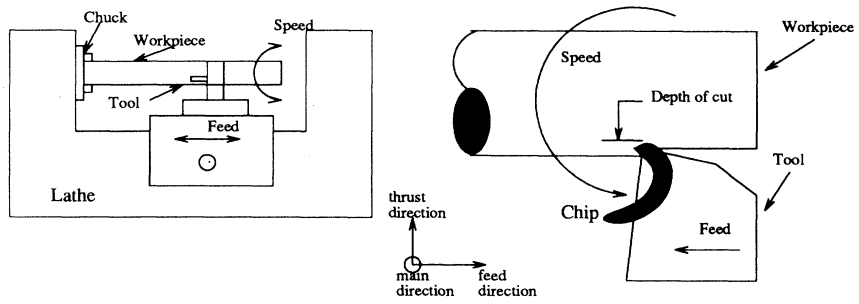

FIG. 1. Schematic of the turning operation.

merical work [8]. We went on to develop a paradigm to control chatter associated with the turning operation based on chaos theory [9, 10]. The success of our control paradigm has motivated us to obtain experimental evidence for chaos in the turning operation, to develop a model capturing the "global" behavior of the turning dynamics, and to apply that model to control the turning operation.

We noted the lack of systematic experimental evidence for the presence of chaos during the turning operation. Therefore, as a first step in this direction, we performed preliminary experiments and collected on-line sensor signals. Then we computed various types of fractal dimensions of these time-series data [11]. The characteristic trend of the capacity dimension indicated that the turning dynamics is chaotic. Parenthetically, we note that the finiteness of fractal dimensions does not necessarily imply the presence of a low-dimensional chaotic attractor. This is more true in the case of fractal dimensions computed from sparse data sets.

The presence of chaos needs to be confirmed by means of rigorous testing procedures on the experimental data from the on-line sensors, and we selected three: (i) a statistical hypothesis test called the *surrogate-data test* [12], (ii) a statistical test called the *quasiperiodicity test* to establish the presence or absence of quasiperiodicity, and (iii) the familiar Lyapunov exponents test [13]. The rationale behind performing these tests in that order will be clear from the implementation details and the results from each stage of implementation presented in Sec. III. Because sensor signal dynamics is reasonably synonymous with the dynamics of turning operation, our conclusions regarding the sensor signals may be extended to actual machining. In this communication, we report the methodology, implementation details, and the results of the three testing procedures.

II. METHODOLOGY

The testing methodology consisted of conducting experiments and obtaining sensor signals therefrom, and establishing evidence for chaos in the time-series data by performing (a) the surrogate-data test, (b) the quasiperiodicity test, and (c) the Lyapunov exponents test.

Experiments were conducted on a 20 HP LeBlond heavy duty lathe. Three different on-line sensors were used: (i) a 3-axis Kistler Z3392/b piezoelectric dynamometer for measuring cutting, feed, and thrust forces; (ii) two PCB accelerometers to measure vibration signals along main and feed directions; and (iii) a SE-900 MWB wide bandwidth AE sensor to measure RMS AE signals. The force sensor signals were sampled at 3 kHz frequency, vibration signals at 26 kHz, and acoustic emission signals at 1 MHz. The workpieces were made of 36 in.$\times\phi$ 7 in. SAE 6150 Cr-V steel, and the tool inserts were K420 uncoated carbide grade with geometric specification SPG-422.

A 5×5 full factorial experimental design consisting of speed (100, 130, 160, 190, and 220 feet/min), and feed (0.0064, 0.0088, 0.0112, 0.0136, and 0.0154 in./rev) was used. The depth of cut was kept constant at 0.05 in. At every design point, a fresh cutting edge was used to perform the turning operation. During every machining operation, time-series data of length 4096 were collected from sensor signals at regular intervals until the tool wore down. This experiment resulted in 650 scalar data sets. The two tests mentioned earlier were conducted on these data sets. Incidentally, time-series data of length > 4096 are beyond our experimental capabilities, but those of length 4096 should suffice [12, 14], especially since we are dealing with multidimensional time series.

A. Surrogate-data test

A deterministic chaotic process can produce signals with broadband noise spectra similar to a stochastic process (provided the spectra exist [15]). But a chaotic process is finite dimensional, whereas a random process is infinite dimensional.

The finite dimensionality of chaotic processes is exploited in the surrogate-data test to distinguish between deterministic chaotic and Gaussian stochastic processes. The testing procedure involves three steps.

(i) *Generation of surrogate time series.* Many stochastic time series with the same average power spectral density (PSD) as the original time-series data are generated. We perform a *histogram transformation* [12] of the time series before generating each stochastic time series, thus ensuring that the original time series and the generated stochastic time series have the same Gaussian distribution, thereby preventing any false-positive results. Every stochastic time series generated is subjected to a two-sample Kolmogorov-Smironov test to ensure that the probability distributions of the original time series and the surrogate time-series sets (i.e., the stochastic time series) are similar.

(ii) *Construction of prediction model.* From the given original and surrogate time-series sets, a state vector is constructed using different independent time-series (sensor signals) and/or lag coordinates. Three kinds of prediction models are commonly used: (a) piecewise linear autoregression (AR) model-based predictor; (b) nearest-neighbor-based predictor; and (c) neural network predictor [16, 17, 12]. The model predictions are computed for the original time-series data and every surrogate time-series generated therefrom.

(iii) *Hypothesis testing.* The original time-series data set is hypothesized to be nonlinear and very likely chaotic. The Mann-Whitney rank-sum statistic

$$\Upsilon = \sum_{n=1}^{N_{\overline{E}}} \sum_{m=1}^{N_{\hat{E}}} \Theta(\overline{E}_n - \hat{E}_m) \tag{1}$$

is computed, where $\overline{E}$ denotes the set of decimated [18] prediction errors computed from the original time-series data, $\hat{E}$ is the set of decimated prediction errors on the surrogate data sets, $N_{\overline{E}}$ is the number of samples in $\overline{E}$, $N_{\hat{E}} = MN$ is the number of samples in $\hat{E}$, M is the number of surrogate-data sets generated, and $\Theta(\,)$ is the Heaviside function. For a large sample set $\overline{E}$, the statistic

$$z = \frac{\Upsilon - N_{\overline{E}} N_{\hat{E}}/2}{\sqrt{\frac{1}{12} N_{\overline{E}} N_{\hat{E}} \left(N_{\overline{E}} + N_{\hat{E}} + 1\right)}} \tag{2}$$

follows the standard normal distribution. The magnitude of this z statistic may be used to reject the null hypothesis that there is no significant difference between the magnitudes of the prediction errors of original time series and the surrogate time-series sets. If the prediction errors of the surrogate time-series sets are significantly larger than those of the original time series, then the original time series is nonlinear and possibly chaotic.

B. Quasiperiodicity test

If a given time series (i) passes the surrogate-data test and therefore is established as being nonlinear, and (ii) has one or more dominant periods superposed on a seemingly random reponse, then it is very likely to be quasiperiodic, though it may be chaotic instead. In this section a statistical test is developed to confirm whether a given time series is (i) low-dimensional chaotic or (ii) quasiperiodic contaminated by Gaussian noise. This test relies on the difference in the representations of quasiperodic and chaotic signals.

1. Quasiperiodic response

An elementary quasiperiodic system response may be represented by

$$x(t) = a_1 \cos(\omega_1 t) + a_2 \cos(\omega_2 t), \tag{3}$$

where $x(t)$ is the state vector, a_1 and a_2 are two amplitude vectors, and ω_1 and ω_2 are mutually incommensurate frequencies (i.e., $\frac{\omega_1}{\omega_2}$ is an irrational number). The frequency spectrum of the quasiperiodic response (3) has only two peaks, corresponding to ω_1 and ω_2 [19]. Furthermore, the Poincaré section plot of the state vector $x(t)$ shows $\frac{2\pi}{\omega_2}$-periodic orbits when the strobe frequency is set at ω_1.

But discrete responses cannot be represented by the right side of (3) which is based on incommensurate frequencies; hence, alternate representations have to be adopted by us. A common representation is

$$x(t) = U(t, 0)x(0), \tag{4}$$

where the time evolution operator

$$U(t, \zeta) = \sum_{n,m} A_{nm} e^{i(n\omega_1 + m\omega_2)(t-\zeta)}, \tag{5}$$

n and m being integers. Thus, the Fourier spectrum of $x(t)$ consists of a dense set of frequencies. Only a few matrices A_{nm} are sufficient to represent many quasiperiodic responses reasonably accurately; but a large number of A_{nm} are needed if the underlying dynamics is chaotic [20]. This enables a quick distinction between a quasiperiodic and chaotic systems.

The representation [(4) and (5)] has certain limitations. If a particular quasiperiodic response appears very complicated, its representation may require a dense set of A_{nm}, hence rendering distinction based merely on frequency spectra incorrect. Badii and Meier have shown [20] that the system response as perceived from a Poincaré section plot may resemble an aperiodic or chaotic response, and even the correlation function evaluated over a small time interval might appear chaotic. In such instances, *double Poincaré section plots* can be used to identify the correct system behavior [20]. Furthermore, system noise has not been accommodated in (4) and (5).

Therefore, we propose that a quasiperiodic response is better represented as the quantized response

$$x(t) = \sum_{n \in W} A_n \sin(\omega_n t + \phi_n) + \epsilon(t), \tag{6}$$

where W is the set of indices of the *codebook* frequencies ω_n obtained by performing a *transform vector quantization* (TVQ) [21] of the given signal using a Gaussian window function in the frequency domain, A_n are the independent and normally distributed amplitude vectors, while $\epsilon(t)$ is an autocorrelated stationary stochastic process.

The representation (6) can be modified to analyze measured time series (which are necessarily discrete). Let $y(k)$ be the measured state vector at time $t = kT$, where T is the sampling period and k is an integer. Its predictor may be obtained from (6) using a multivariate ARMA (auto regressive and moving average) model [22] as

$$w(k+1) = \Phi w(k) + \Psi e(k), \tag{7}$$

where $w(k) = \epsilon(kT)$, Φ and Ψ are the ARMA model coefficients, and $e(k)$ is the normally distributed prediction error.

2. Chaotic response

Following the findings of Baker *et al.* [23], we can state that chaotic responses cannot be parsimoniously represented by (6). But, nonlinear models such as neural networks may be used for representation and prediction of chaotic time series [17]. The methodology of developing a neural network based representation of a chaotic response is as follows.

From a given time series, we may set up the input (i.e., training and/or testing) patterns based on the optimal embedding dimension obtained using other methods (e.g., surrogate-data test). The output of the neural network consists of the last component of $y(k+1)$. After training the neural network using selected training patterns, the same patterns may be used for testing. Alternatively, patterns extracted from a second experiment conducted at the same control parameter combination and tool wear level may be used for testing. Neural network model prediction errors $\tilde{e}(k)$ may be obtained by testing the trained network.

3. Testing procedure

A given time series is first assumed to be quasiperiodic and modeled using (6) and (7)—prediction errors $e(k)$ are thus obtained. Next the time series is assumed to be chaotic and represented using the neural network model—to obtain $\tilde{e}(k)$.

The two sets of prediction errors are used to verify the null hypothesis

$$H_0: \quad \mu_{e-\tilde{e}} = 0, \tag{8}$$

where $\mu_{e-\tilde{e}}$ is the population mean of $e(k) - \tilde{e}(k)$. If H_0 holds, the time series is quasiperiodic. The alternative hypothesis may be stated as

$$H_1: \quad \mu_{e-\tilde{e}} \geq 0. \tag{9}$$

If H_1 holds, the time series is very likely to be chaotic. Hypothesis testing may be carried out using the normal statistic

$$z^* = \bar{\kappa} \Big/ \sqrt{\frac{s_\kappa^2}{N_s}}, \tag{10}$$

where N_s is the sample size (i.e., the number of testing patterns), $\bar{\kappa}$ is the sample mean of $\kappa = e - \tilde{e}$, and s_κ^2 is its sample variance.

Thus the prediction errors obtained from both assumptions are compared, and a normal test is used to either confirm or reject the hypothesis of the absence of quasiperiodicity and presence of chaos.

C. Lyapunov-exponents test

If a given time series fails the null hypothesis (8), it is not quasiperiodic (whether contaminated by Gaussian noise or not) and is very likely to be chaotic. But, if (i) the length of the time series is not large enough and (ii) the nature of quasiperiodicity is complicated (for instance, arising from multiple bifurcations), not much confidence can be placed on the results of Sec. II B. Therefore, the Lyapunov-exponents test has to be performed in such situations. Lyapunov exponents are the best quantifiers of chaos in a dynamical system. They signify the divergence rate, along a particular direction, of small perturbations to an orbit.

Suppose the state of the system is sampled at times $t = kT$, $0 \leq k \leq N$. For simplicity, let us consider a *one-dimensional* time series $y(k)$ and the corresponding nonlinear map

$$y(k+1) = \Im(y(k)), \tag{11}$$

where $\Im(\,)$ is a nonlinear mapping function.

The evolution $\Delta y(k)$ of a small perturbation $\Delta y(0)$ of the initial state $y(0)$ is given iteratively by

$$\Delta y(k+1) = J\Im^k(y(0))\Delta y(0). \tag{12}$$

Here, J stands for the Jacobian such that $J\Im^k(y(0)) = (\frac{d\Im(y)}{dy})_{y=y(k)}$, and

$$\lim_{k\to\infty} e^{-k\lambda}\, J\Im^k(y(0)) = 1, \tag{13}$$

where λ is the global Lyapunov exponent [24] of the attractor represented by $y(k)$.

This concept of Lyapunov exponents may be extended to a d-dimensional time series, the integer $d \geq 1$. In that case, the single λ must be replaced by a diagonal matrix containing d Lyapunov exponents computed from the eigenvalues $\nu_m(k)$ of the positive semidefinite matrix $[J\Im^k(y(0))]^T[J\Im^k(y(0))]$ as

$$\lambda_m = \lim_{k\to\infty} \frac{1}{2k} \log_e[\nu_m(k)] \quad (m = 1, ..., d), \tag{14}$$

for a given $y(0)$. The superscript T denotes the transpose.

A system is dissipative if the sum of the d Lyapunov exponents is less than zero, and it is chaotic when at least one of the Lyapunov exponents is positive. The presence of positive Lyapunov exponents is regarded [13] as a reliable confirmatory test for the presence of chaos.

However, the unavoidable presence of noise or other contamination tends to increase the Lyapunov exponents. Therefore, the measured signal has to be separated from noise. If the time series were linear, signal extraction using a narrow-band window could be sufficient and all necessary analyses could be carried out in the Fourier domain. But Fourier analysis is of little avail for a nonlinear time series.

The crux of the problem in the latter case is to characterize the given signals by identifying and separating components originating from various sources. We employ a wavelet transform to perform signal separation. The procedure to accomplish this transform has been described by Dai *et al.* [25]. Interested readers are also referred to the excellent manual on wavelet transforms written by Naylor and Silverman [26].

The following assumptions underlie the application of

wavelet transforms for signal separation: (i) All signal components collected during the turning operation with *zero* depth of cut are extraneous and, therefore, must be calibrated out to establish baselines; (ii) the noise floor (the power of undesired signals) is low compared with that of the desired signals; (iii) signal mixing is not heavy. Under this set of assumptions, wavelet transforms are more accurate compared with Fourier transforms. This is because the effect of linearization and thresholding in wavelet transforms is localized, whereas the effect is global in Fourier transforms [21].

Let $\varepsilon_{\rm th}$ the denote the threshold value below which all coefficients of the wavelet tranform of the time series are neglected [26]. If ε_m is the measured total energy contained in *zero* depth-of-cut turning, after assuming the presence of only white noise, we set the threshold

$$\varepsilon_{\rm th} = \frac{\varepsilon_m}{2^N}. \tag{15}$$

Using this threshold value, wavelet transforms of the filtered signal may be carried out and the Lyapunov exponents calculated.

III. IMPLEMENTATION AND RESULTS

Our implementation phase started with graphical (Poincaré) analysis of the measured time-series. The results obtained therefrom were confirmed using the surrogate-data test, the quasiperiodicity test and the Lyapunov exponents test.

A. Graphical analysis

The individual sensor signals were grouped into three categories corresponding to: (i) the force sensor system, (ii) the vibration sensor system, and (iii) acoustic emission. Graphical analysis was performed on each of these three groups.

1. Force system

Representative time-series data for the three forces are shown in Fig. 2. The first column of the figure shows the time-series data obtained during an experiment performed with a fresh cutting tool, at a cutting speed of

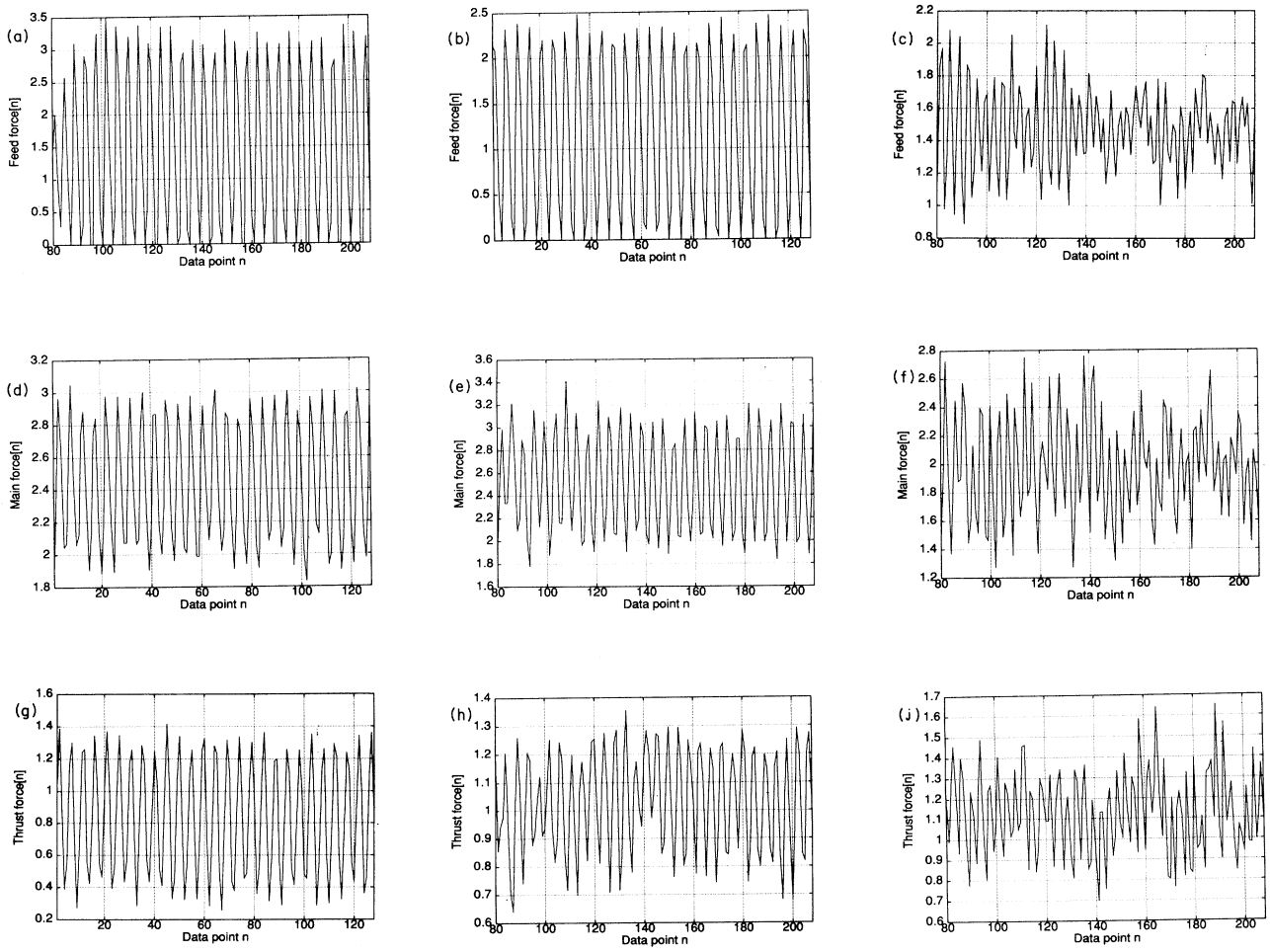

FIG. 2. Time-series plots of force sensor signals: The first column shows plots for a fresh tool, the second column for a partially worn tool, and the third column for a fully worn tool. [Cutting speed = 130 feet/min, feed = 0.0088 in./rev; flank wear = 0.0000 in. (fresh tool), 0.006 in. (partially worn), 0.0175 in. (fully worn)].

130 feet/min and feed of 0.0088 in./rev. The first figure in the first column is the time-series plot of feed force signals. Below the feed force plot are the main force signal plot and thrust force plot, respectively. The time series appear almost periodic with a dominant period of approximately four time steps.

The second and the third columns in Fig. 2 show the time-series plots when the tool is partially worn (0.006 in. flank wear) and fully worn (0.0175 in. flank wear), respectively. The plots reveal that as the tool wear progresses, the signal pattern becomes more irregular. This may be attributed to the presence of multiple secondary cutting edges as well as to the irregular sliding surfaces developed by tool wear. However, the dominant time period remains the same: approximately four time steps. This result was confirmed from the analysis of the corresponding (a) correlation plots and (b) mutual information plots.

Next, we developed the Poincaré section plots of the force system at different tool wear levels. A Poincaré section plot essentially is a strobe plot corresponding to the dominant time period [27]. We chose the Poincaré section strobe period $\tau = \ell T$ based on mutual information and correlation plots, which rendered the selection of ℓ fairly robust [13]. The value $\ell = 4$ was chosen thus for Poincaré section plots, some examples of which are shown in Fig. 3. The plots showed that the essential system dynamics is reasonably captured within a three-dimensional manifold. However, we have noted that, when the cutting tool wear is high, the additional dynamics introduced due to the secondary cutting edges and the flank surface rub-

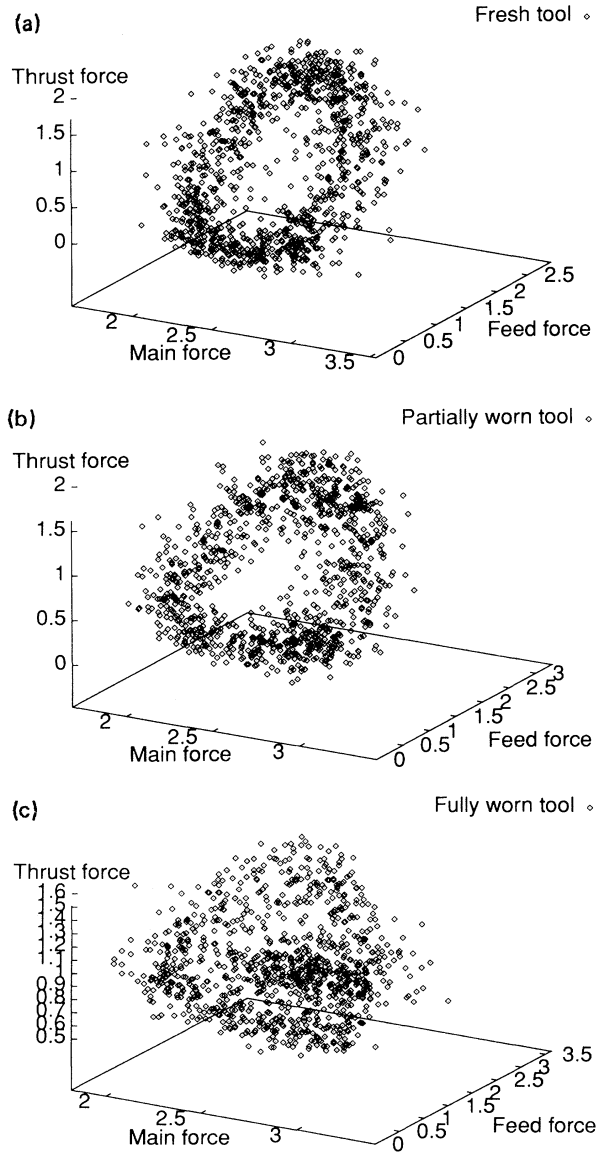

FIG. 3. Poincaré section plots of the force sensor system. [Cutting speed = 130 feet/min, feed = 0.0088 in./rev; flank wear = 0.0000 in. (fresh tool), 0.006 in. (partially worn), 0.0175 in. (fully worn).]

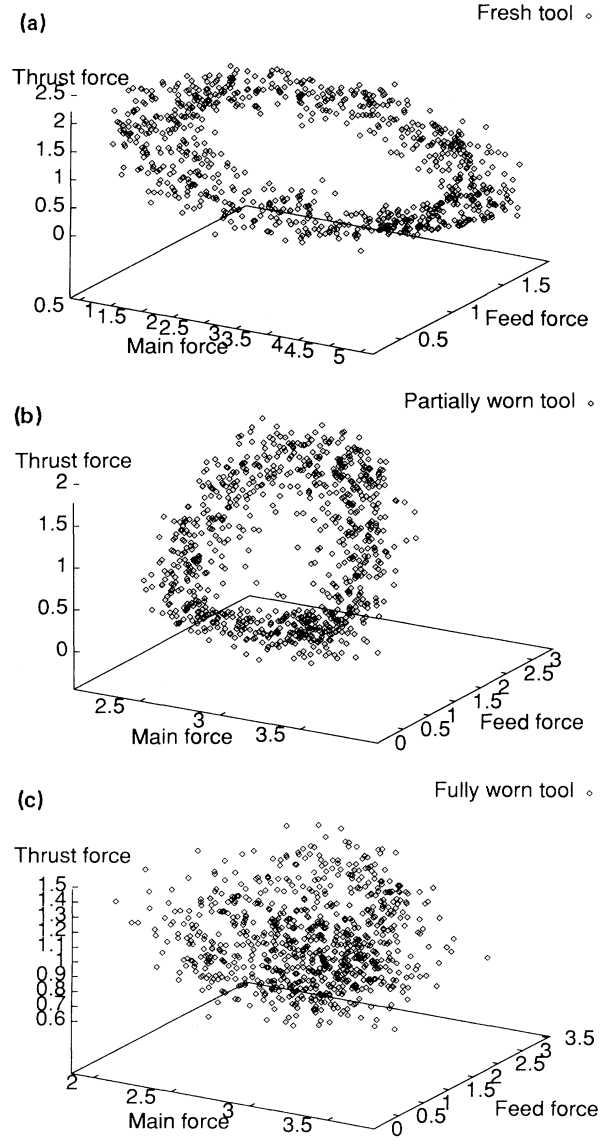

FIG. 4. Poincaré section plots of the force sensor system at a different control parameter setting. [Cutting speed = 160 feet/min, feed = 0.0064 in./rev; flank wear = 0.0000 in. (fresh tool), 0.011 in. (partially worn), 0.0181 in. (fully worn).]

bing action lead to complications that are not completely revealed in three-dimensional plots [11]. This fact is also confirmed by the double Poincaré section plots discussed later. The Poincaré section plots of the force system at a different control parameter setting, i.e., cutting speed of 160 feet/min and feed of 0.0064 in./rev are shown in Fig. 4. On comparing Figs. 3 and 4, as well as from numerous other Poincaré section plots, we conclude that the dynamics does not change significantly over the working range of the control parameters.

We drew lag plots at different wear levels, as exemplified by Fig. 5. Lag plots correlate the kth state to the $(k+r)$th state, where r is the lag [14]. Lag of $r = 4$ was used for plots. The first column shows the lag plots of feed force ($F_f[k]$ versus $F_f[k-4]$), and main force ($F_m[k]$ versus $F_m[k-4]$) for a fresh tool, with $k = 4, 8, 12, \ldots$. The second column has the same plots drawn for a worn tool. These plots also confirm the presence of a distinct structure underlying the sensor signal data. In particular, the underlying structure corresponds to either deterministic chaos, quasiperiodicity interfered with Gaussian contamination, or "noisy" periodicity. The exact identity of the underlying structure can be ascertained from the quantitative analytical procedures outlined in Sec. II.

2. *Vibration system*

Representative time-series data for the vibration along the main and feed directions are shown in Fig. 6. These and other plots show that the dominant time period of the vibration system is approximately five time steps, i.e., $5T$.

The Poincaré section plots of the vibration system (exemplified in Fig. 7) reveal the presence of a low-dimensional attractor. As for the force system, the Poincaré plot of the vibration system is not very sensitive to changes in the control parameter setting; however, it is affected by the cutting tool wear. Lag plots confirmed these observations.

We also performed graphical analysis of acoustic emission signals. The chief sources of acoustic emission in turning operations are the plastic deformation zones [1]. Acoustic emission is extremely sensitive to microlevel

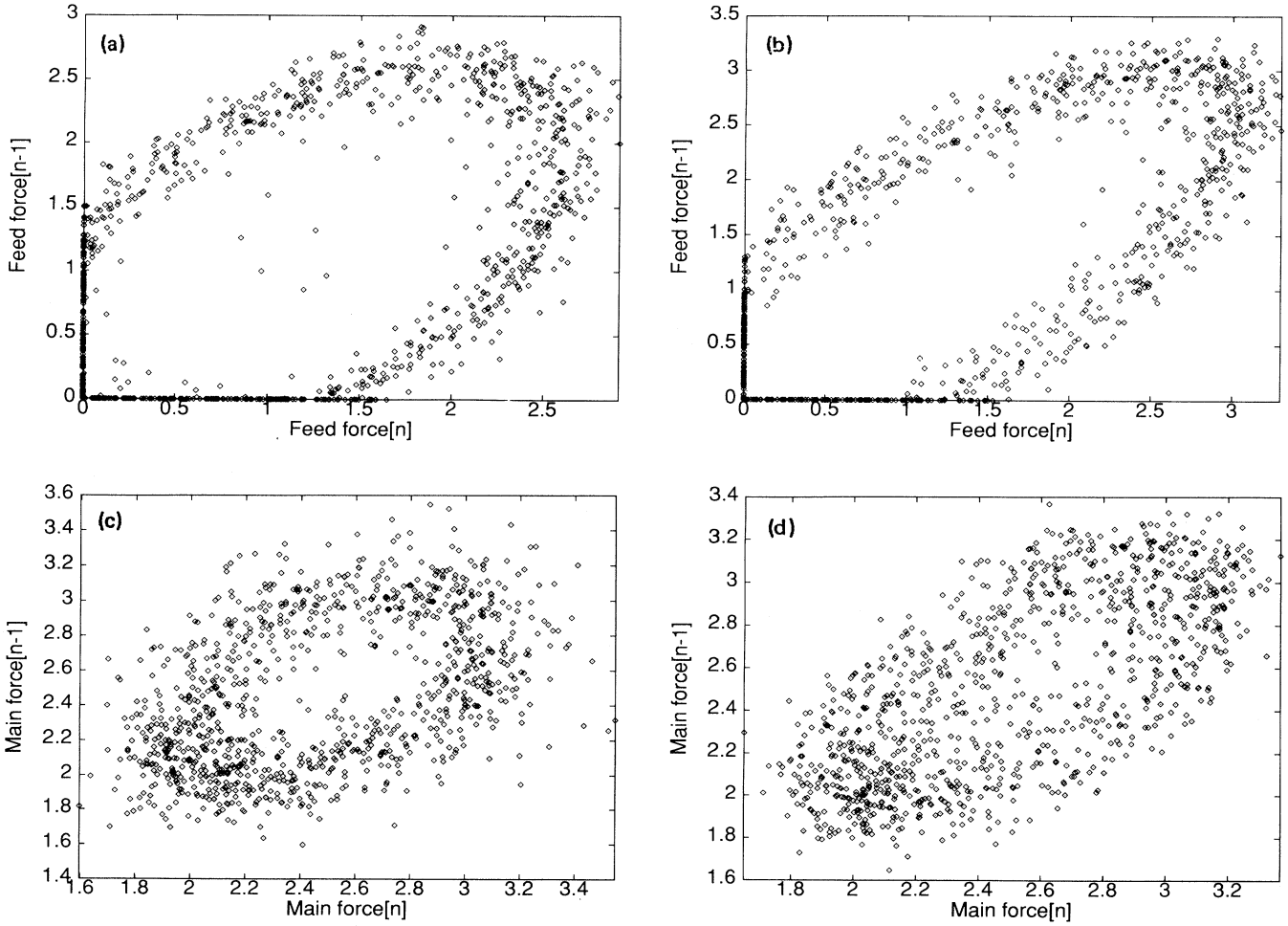

FIG. 5. Lag plots of force sensor data, $n = k/4$, $k = 4, 8, 12, \ldots$. The first column shows plots for a fresh tool, the second column for a fully worn tool. [Cutting speed = 130 feet/min, feed = 0.0088 in./rev; flank wear = 0.0000 in. (fresh tool), and 0.0175 in. (worn tool).]

variations in the turning process. Sample time-series plots are shown in Fig. 8. The acoustic emission signal is highly time varying and hence requires enormously high sampling rates and precision levels to obtain phase portraits with a reasonable structure. The sampling rate and precision requirements are beyond our present experimental capabilities, so we ignored acoustic emission data.

B. Fractal dimension estimation

In order to carry out the three tests described in Sec. II, first we needed to determine various fractal dimensions which gave initial estimates of the possible embedding dimensions to use. Fractal dimensions of the Poincaré maps of individual sensor signals were determined using a fast box-counting algorithm developed by Liebovitch and Toth [28]. Individual sensor signal data sets, each of length $N = 4096$, were used to compute the fractal dimensions. The variation of the correlation integral with the radius of the hypersquare box is shown in Fig. 9(a). The plots are linear over three to four scales of the box radius.

The variations of capacity, correlation, and information dimensions with the embedding dimension were studied. For $d_E \geq 6$, the state space usually turned out to be sparse for accurate estimation. Two representative plots to exemplify this conclusion are shown in Fig. 9(b). Figures 9(a) and 9(b) correspond to the data obtained from two replications of experiments performed with a fresh tool under the following randomly chosen parameter settings: cutting speed = 160 feet/min, feed = 0.0136 in./rev, depth of cut = 0.05 in.

In order to ascertain the sufficiency of 4096 data points for calculating the fractal dimension values, fractal dimensions of the vector time series obtained from two and then three "close" parameter settings were determined under different embedding dimensions. The averages taken over various parameter settings and tool wear values are reported here. Let us recall from the results of graphical analysis in Sec. III that the dynamics of the force-and-vibration system did not vary significantly with parameter settings. Thus, our methodology of combining the data sets is reasonably justified.

Furthermore, this procedure for estimating fractal dimensions automatically accounted for the higher order dynamics imposed by signal contamination. Due to the presence of contamination, fractal dimension versus embedding dimension graphs showed a reasonably well-defined change of slope, especially at low tool wear levels. As we are not interested in characterizing this complicated dynamics at this stage of our effort, we limited our estimations up to $d_E \leq 6$.

The fractal dimension estimator we used [28] is designed to calculate the complete fractal dimension spectrum; however only the capacity dimensions are stated in this paper. Various sensor data had average fractal (capacity) dimensions in the range 1.58–1.67, as shown in Table I. This implies that the fractal dimension of the attractor of the dynamics is in a small neighborhood of 2.63 (for a deterministic system, $D = D_p + 1$, where D is the dimension of the attractor and D_p is the dimension of the Poincaré section).

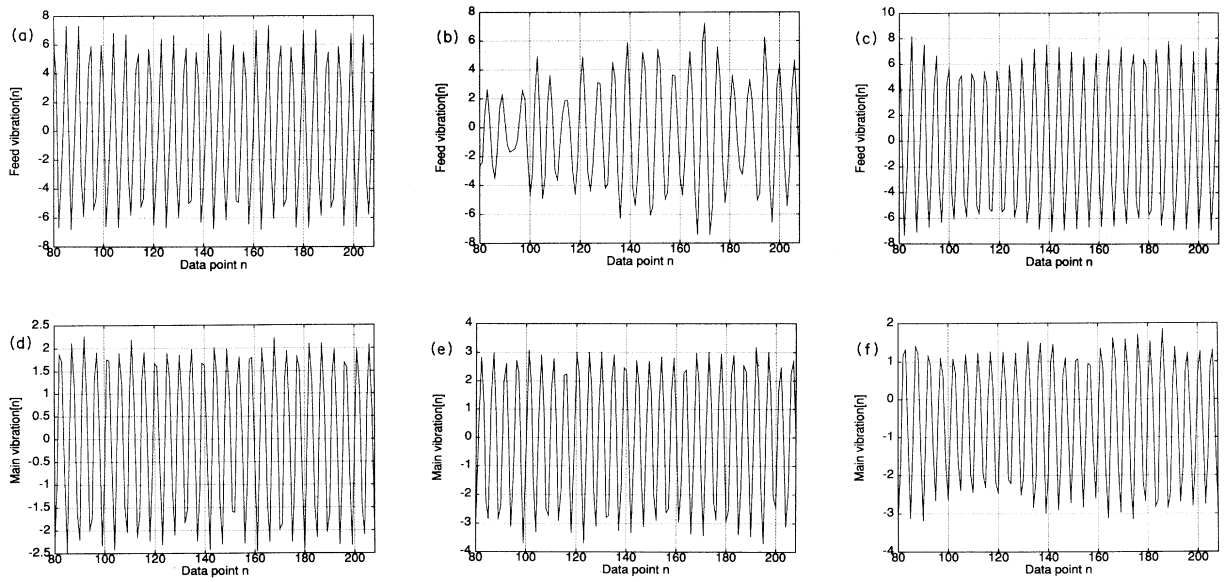

FIG. 6. Time-series plots of vibration sensor signals: Column 1 shows plots for a fresh tool, column 2 for a partially worn tool, and column 3 for a fully worn tool. [Cutting speed = 130 feet/min, feed = 0.0088 in./rev; flank wear = 0.0000 in. (fresh tool), 0.006 in. (partially worn), 0.0175 in. (fully worn).]

TABLE I. Estimated capacity fractal dimension (D_p) for four sensor signals.

Sensor	Fractal dimension D_p
Main force sensor	1.65
Feed force sensor	1.62
Main vibration sensor	1.67
Feed vibration sensor	1.58

C. Surrogate-data test

The surrogate-data test was conducted on the equispaced time-series data representing the sensor signals obtained from actual experiments. The average *decorrelation time* of the data was eight time steps. The first minimum of the *mutual information function* [13] for different data sets was found to be four time steps for force

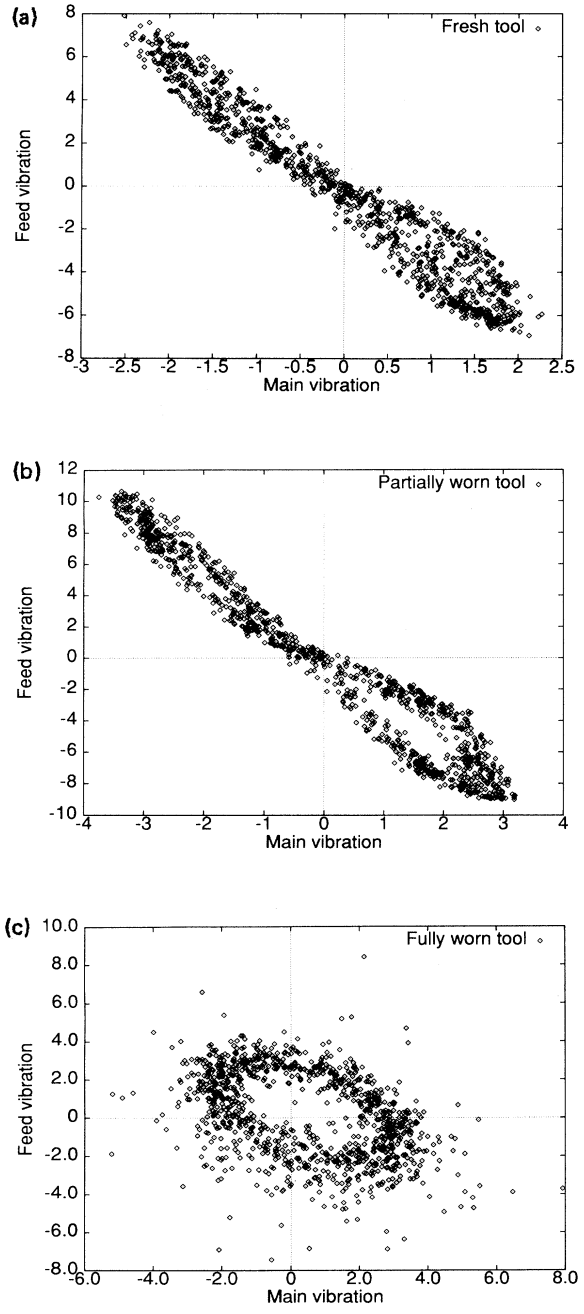

FIG. 7. Poincaré section plots of the vibration system. [Cutting speed = 130 feet/min, feed = 0.0088 in./rev; flank wear = 0.0000 in. (fresh tool), 0.006 in. (partially worn), 0.0175 in. (fully worn).]

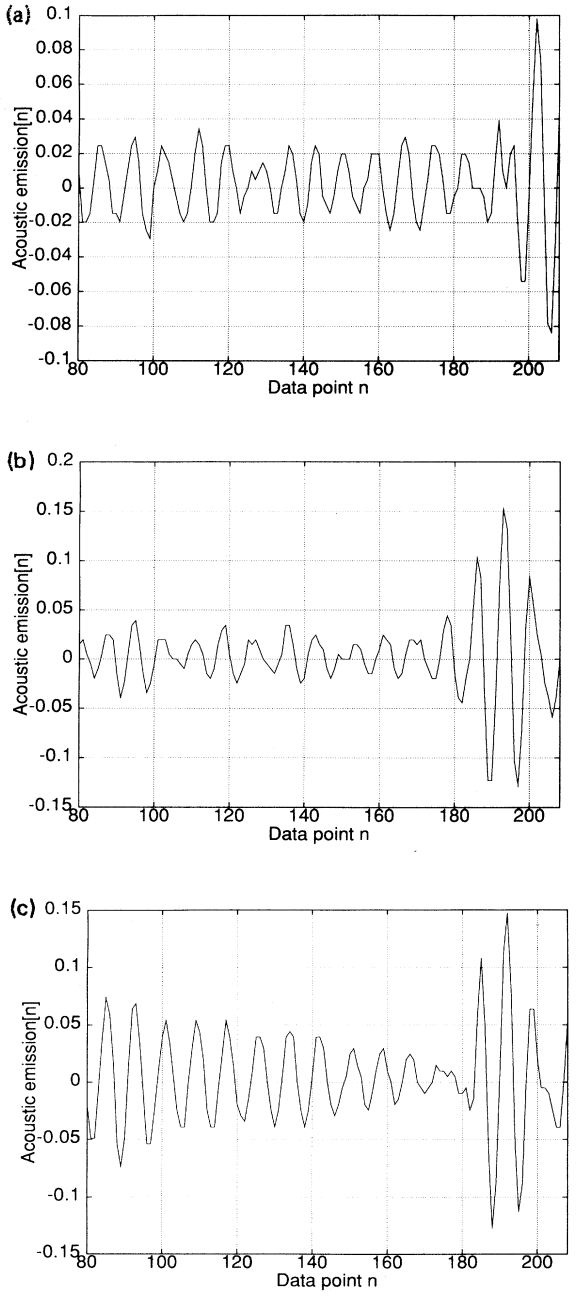

FIG. 8. Time-series plots of acoutic emission sensor for a fresh tool (top), a partially worn tool (middle), and a fully worn tool (bottom). [Cutting speed = 130 feet/min, feed = 0.0088 in./rev; flank wear = 0.0000 in. (fresh tool), 0.006 in. (partially worn), 0.0175 in. (fully worn).]

TABLE II. Results of the surrogate-data test for a piecewise linear AR model.

Sensor	Average z statistic				
	$d_E = 2$	$d_E = 3$	$d_E = 4$	$d_E = 5$	$d_E = 6$
Main force sensor	−2.35	−3.34	−6.12	−6.05	−6.01
Feed force sensor	−3.13	−3.55	−7.23	−6.83	−4.88
Main vibration sensor	−4.23	−5.12	−10.01	−9.13	−6.95
Feed vibration sensor	−2.88	−4.17	−7.45	−7.42	−6.23

sensor signals and five time steps for vibration sensor signals. The mutual information function leveled off after nine time steps.

The first 2048 data points from the main force, feed force, main vibration, and feed vibration sensors were used for the test. Scalar time-series data from individual sensors were tested. The tests were conducted for embedding dimensions d_E ranging from 1 to 6. Corresponding to the largest frequency of interest, time delays of one to six time steps were used, and the prediction interval of four time steps in the reconstructed state vector (approximately half of the first significant minimum of the mutual information function) was used. Twenty surrogate data sets were generated.

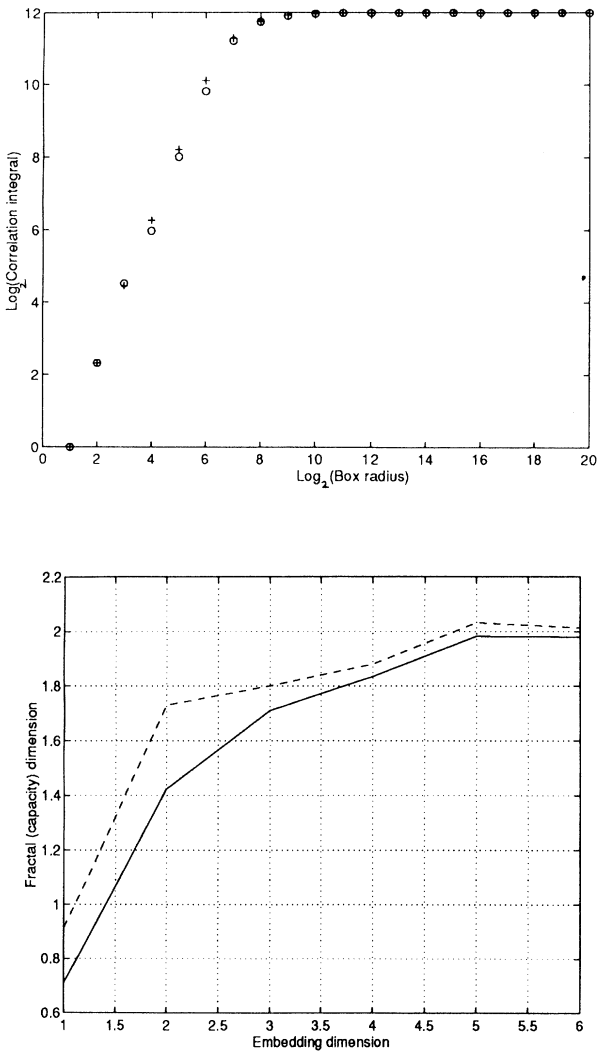

FIG. 9. Representative data for (a) variation of correlation function with box radius, (b) variation of fractal dimension with embedding dimension for two experimental runs conducted using a fresh tool. (Cutting speed = 160 feet/min, feed = 0.0136 in./rev.)

Prediction errors were computed for the original time series and the surrogate time series. Hypothesis testing was performed for three prediction models used: (i) piecewise linear AR model, (ii) nearest-neighbor-based predictor, and (iii) neural network predictor. The Mann-Whitney rank-sum statistic was then obtained. Let us note that the values of $z \leq -2.33$ correspond to a 99% confidence level of stating that prediction errors of the original data sets are significantly lower than those of the surrogate data sets, implying that the original time series is indeed nonlinear [29] and possibly chaotic [12].

The results of the surrogate-data test for linear, nearest-neighbor, and neural network predictor models are presented in Tables II, III, and IV, respectively. The results show that the measured time-series data correspond to a chaotic or nonlinear process because the *minimum* z statistic for all sensors is well below the 99% confidence level of −2.33. In other words, the vibrations of the cutting tool, the forces, and hence the turning dynamics, are nonlinear and possibly chaotic. Furthermore, from Table II, it is evident that the predictability of the measured state vector is high if $d_E = 4$ because the minimum z statistics occur when $d_E = 4$. This result is in consonance with the value of the optimal embedding dimension obtained using fractal dimensions [30]. Moreover, it may be noted from Table V that the prediction errors resulting from the neural network model was about 10% lower than those from the local linear model. This reinforces the confirmation that the measured time-series data are nonlinear.

TABLE III. Results of the surrogate-data test for the nearest neighbor prediction model ($d_E = 4$). Minimum z statistics occurred at $d_E = 4$.

Sensor	Average z statistic
Main force sensor	−5.78
Feed force sensor	−7.19
Main vibration sensor	−6.91
Feed vibration sensor	−4.55

TABLE IV. Results of the surrogate-data test for the neural network prediction model ($d_E = 4$). Minimum z statistics occurred at $d_E = 4$.

Sensor	Average z statistic
Main force sensor	−14.23
Feed force sensor	−11.94
Main vibration sensor	−17.06
Feed vibration sensor	−9.89

TABLE V. Percentage improvement in the prediction error from the neural network model over the piecewise linear model at $d_E = 4$.

Sensor	Percentage improvement
Main force sensor	11.3
Feed force sensor	6.7
Main vibration sensor	10.1
Feed vibration sensor	8.4

D. Quasiperiodicity test

The results of the graphical analysis and the surrogate-data tests have established the nonlinearity of the turning dynamics. Specifically, the turning dynamics could be either (i) low-dimensional chaos or (ii) quasiperiodicity interfered with by an autocorrelated stochastic process. Therefore, we went on to devise a quasiperiodicity test.

We first visualized the measured data using double Poincaré section plots. First we computed the second significant period of the original time-series data (which turned out to correspond to the second major minimum of the mutual information function and the second dominant frequency), and recorded a point on the Poincaré section plot only if the current time index was close to an integral multiple of the second dominant period. The recorded data points corresponded approximately to the multiples of 63 time indices. Figure 10 is a representative double Poincaré section plot of the force system drawn from data collected with a fresh tool at the following parameter settings: speed = 160 feet/min, feed = 0.0136 in./rev, and depth of cut = 0.05 in. It reveals a definite structure which is not merely of type (ii).

A statistical test to correctly characterize the turning dynamics from the given time-series data has been outlined in Sec. II B. We particularly noted that the attractor appears to be a quasiperiodic two-dimensional torus (as seen from the Poincaré section plots), as well as a three-dimensional torus (as seen from the double Poincaré plot). We therefore used a quantization rate [21] of 4 to perform the TVQ. From the quantized response obtained from (6), four-dimensional vectors $w(k)$ were computed. Our iterative algorithm ensured that $w(k)$ was a stationary stochastic sequence. Using $w(k)$ an ARMA model was developed, and the prediction errors $e(k)$ were obtained therefrom.

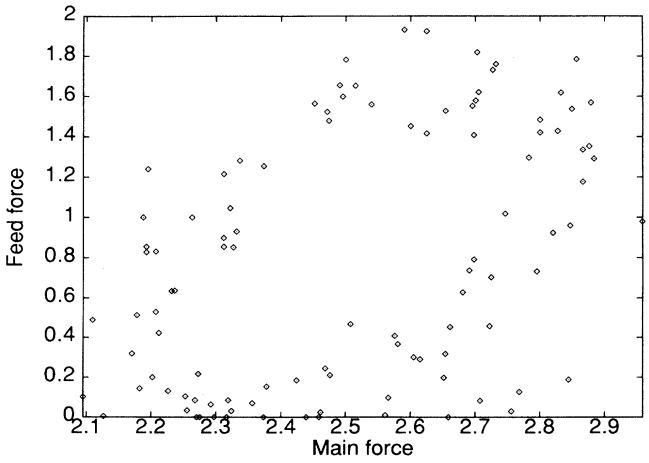

FIG. 10. Double Poincaré section plot of force system for a fresh tool. [Cutting speed = 160 feet/min, feed = 0.0136 in./rev.]

A two-layer time-delay neural network with six input nodes [four input nodes corresponding to the components of $y(k)$, the fifth for speed, and the sixth for feed], six hidden nodes and a single output node was trained with 2000 time-delayed patterns. Error backpropagation algorithm [11] was used for training the neural network. Then the neural network was tested using the same 2000 patterns plus 800 additional patterns and the prediction errors $\tilde{e}(k)$ were computed. Parenthetically, we note that this testing strategy prevents overtraining the neural network.

The prediction errors $e(k)$ and $\tilde{e}(k)$ were used to verify the null hypothesis (8) with $N_s = 24\,500$ and $z^* = 3.13$. Computed results showed that the hypothesis (8) was rejected at a 95% confidence level but accepted at a 99% level. This explains why at first glance the attractor of the turning dynamics may appear to be quasiperiodic, but actually it is not so. Perhaps in some regions of the control parameter space, the attractor could be quasiperiodic with a toroidal shape, but it certainly is not so at the control parameter values corresponding to practical cutting conditions.

We therefore conclude that, for the control parameter combinations chosen for our experiments, the turning dynamics may be more accurately described as a low-dimensional chaotic process than as a quasiperiodic process interfered with Gaussian contaminants. Furthermore, for certain applications, the response of the turning process may be represented by (6).

Since the quasiperiodicity test failed to confirm the presence of chaos at 99% confidence level, another confirmation test had to be carried out. The final confirmation of chaos was accomplished using the Lyapunov-exponents test.

E. Lyapunov-exponents test

The methodology outlined in Sec. II C was followed to calculate Lyapunov exponents of the Poincaré section

TABLE VI. Results of the Lyapunov-exponent test. All entries except one are < 2.0, the sole exception arising due to inadequate filtering.

Sensor	Dominant Lyapunov exponent				
	$d_E = 1$	$d_E = 2$	$d_E = 3$	$d_E = 4$	$d_E = 5$
Main force sensor	0.7208	0.5216	2.2233	1.9885	1.7843
Feed force sensor	0.3017	1.0999	1.9949	1.8947	1.7489
Main vibration sensor	0.9216	1.5689	1.8934	1.9931	1.8309
Feed vibration sensor	1.9341	0.7199	1.7263	1.9238	0.8356

plots, which may be referred to as the Lyapunov numbers by some. First, the *zero* depth-of-cut signal was obtained. Its energy content ε_m was found to be 0.062 times the average energy ($\approx 2^{N-1}$) during the regular experiments, and the threshold ε_{th} was computed using (15) to be 0.031.

Next, the Lyapunov exponents of the measured time-series sensor signals were determined using the methodology outlined by Abarbanel *et al.* [13]. It involves expressing the overall divergence of a trajectory as a product of local divergences and then computing the eigenvalues of the product through QR decomposition [31]. The computed results are shown in Table VI. The dominant Lyapunov exponents are < 2.0 for $1 \leq d_E \leq 5$; in particular, they hover between 1.89 and 2.00 when $d_E = 4$, the optimal embedding dimension. It follows therefrom that the dynamics of turning operation exhibits low-dimensional chaos. The values of the Lyapunov exponents are slightly higher than those usually regarded as being characteristic of low-dimensional attractors. However, we conjecture that the slightly higher values may be due to inadequate filtering which has possibly allowed some noisy components to pass through.

The results of the Lyapunov-exponents test imply that piecewise linearization of the turning dynamics may be appropriate for adequate control schemes.

IV. CONCLUDING REMARKS

Using the battery of tests performed, the turning operation on a lathe was found to exhibit low-dimensional chaos. The Poincaré plots of the force and vibration sensors of the cutting tool revealed a definite structure, thus establishing the presence of a low-dimensional attractor.

We did not state the interval estimates (i.e., error bars) of fractal dimensions in order to be concise in our reporting. We conjecture that with the availability of longer time series in the future, the results of graphical analysis and the quantitative tests will be more convincing. Furthermore, we found that the process dynamics is on the edge of chaos because the Lyapunov exponents are not very large. Therefore the turning dynamics may be successfully learned by computational learning tools such as neural networks [9, 11]. These neural networks can be used for the on-line estimation of cutting tool wear [32] and for chatter control [9] in turning.

To summarize our findings, the turning operation on a lathe was statistically confirmed, perhaps for the first time, to exhibit low-dimensional chaos, leading to the conclusion that it is controllable. The surrogate-data test and the quasiperiodicity tests showed that the turning operation is predominantly chaotic, whose low dimensionality was established by the Lyapunov-exponent test. As these results were established from actual experiments, the invariants of the dynamics such as the fractal dimensions—for the given range of process parameters—are realistic, and may be used to develop practical models to control the turning operation. This understanding is in consonance with Ruelle's recent survey [5] of chaos modeling of diverse physical phenomena. Presently, we are developing a nonlinear dynamics-based theory to explain various physical phenomena that contribute to cutting tool chatter in turning.

ACKNOWLEDGMENTS

We acknowledge the National Science Foundation for supporting this work under NSF Grant No. DDM–9223181.

[1] E. Trent, *Metal Cutting* (Butterworth-Heinemann, Oxford, 1991).
[2] K. Danai and G. Ulsoy, J. Eng. Indust. **4**, 396 (1987).
[3] K. Danai and G. Ulsoy, in *Proceedings of the 1988 ASME American Control Conference, Arizona* (ASME Press, New York, 1988), Vol. 109, p. 1930.
[4] I. Grabec, Phy. Lett. A **117**, 68 (1986).
[5] D. Ruelle, Phys. Today **47** (7), 24 (1994).
[6] P. Bayly and L. Virgin, Phys. Rev. E **50**, 604 (1994).
[7] S. T. S. Bukkapatnam, S. R. T. Kumara, and A. Lakhtakia, IIE Trans. (to be published).
[8] J. Pachner, Comp. Phys. **7**, 68 (1993).
[9] S. T. S. Bukkapatnam, A. Lakhtakia, and S. R. T. Kumara, Spec. Sci. Technol. (to be published).
[10] S. T. S. Bukkapatnam, M.S. thesis, Pennsylvania State University, University Park, PA (1994) (unpublished).
[11] S. T. S. Bukkapatnam, S. R. T. Kumara, and A. Lakhtakia, *Proceedings of Artificial Neural Networks in Engineering 94, Missouri* (ASME Press, New York, 1994).
[12] M. Kennel and S. Isabelle, Phys. Rev. A **46**, 3111 (1992).
[13] H. Abarbanel, R. Brown, and L. Tsimring, Rev. Mod. Phys. **65**, 1331 (1993).
[14] M. Casdagli, Physica D **35**, 335 (1989).

[15] S. Boyd and L. Chua, IEEE Trans. Circ. Syst. **32**, 968 (1985).
[16] A. Tsonis, *Chaos — From Theory to Applications* (Pergamon, New York, 1992).
[17] J. D. Farmer and J. F. Gibson, Physica D **57**, 1389 (1992).
[18] Decimation refers to regular sampling from a set of computed prediction errors and culling of other elements.
[19] F. Moon, *Chaotic Vibrations* (Wiley, New York, 1987).
[20] R. Badii and P. F. Meier, Phys. Rev. Lett. **58**, 1045 (1987).
[21] A. Goldberg, Ph.D. thesis, Stanford University (1993) (unpublished).
[22] M. Kendall and K. Ord, *Time Series* (Edward Arnold, Kent, UK, 1990).
[23] C. P. Baker, M. E. Genaux, and T. D. Burton, in *Dynamics of Time-Varying Systems and Structures*, edited by S. C. Sinha and R. M. Evan-Iwanosky (ASME Press, New York, 1993), p. 195.
[24] S. N. Rasband, *Chaotic Dynamics of Nonlinear Systems* (Wiley, New York, 1990), Chap. 2.
[25] X. Dai, B. Joseph, and R. L. Motard, in *Wavelet Applications in Chemical Engineering*, edited by R. L. Motard and B. Joseph (Kluwer, Boston, 1994).
[26] G. P. Naylor and B. W. Silverman, *Statistical Research Report 93:07* (University of Bath, Bath, UK, 1993).
[27] Reference [24], p. 7.
[28] L. Liebovitch and T. Toth, Phys. Lett. A **141**, 386 (1989).
[29] M. Palus and D. Novotna, *Santa Fe Institute Publication – 94-07-043* (Santa Fe Institute, Santa Fe, 1994).
[30] S. R. T. Kumara, A. Lakhtakia, and S. T. S. Bukkapatnam, *Proceedings of 1994 NSF Grantees Conference, Cambridge, Massachusetts* (Society of Manufacturing Engineers, Dearborn, MI, 1994), p. 171.
[31] G. Strang, *Introduction to Applied Mathematics* (Wellesley-Cambridge Press, Wellesley, MA, 1986).
[32] S. Kamarthi, G. Shankar, P. Cohen, and S. R. T. Kumara, in *Intelligent Engineering Systems Through Artificial Neural Networks*, edited by C. Dagli, S. R.T. Kumara, and Y. C. Shin (ASME Press, New York, 1991), p. 639.